Highly intensified emission of laser-accelerated electrons from a foil target through an additional rear laser plasma

Shunsuke Inoue,* Yoshihide Nakamiya, Kensuke Teramoto, Masaki Hashida, and Shuji Sakabe

Advanced Research Center for Beam Science, Institute for Chemical Research, Kyoto University, Gokasho, Uji, Kyoto 611-0011, Japan and Department of Physics, Graduate School of Science, Kyoto University, Kitashirakawa, Sakyo, Kyoto 606-8502, Japan

(Received 16 May 2016; published 12 April 2018)

Intensification of electrons escaping from an intense laser-produced plasma is demonstrated by using double femtosecond laser pulses. The electron density distribution at the rear surface of a laser-irradiated foil target is controlled by preirradiation to suppress sheath field growth and to expand the plasma into which the fast electrons are released. Consequently, the number of electrons escaping from the plasma that have an energy of 380 keV increases by a factor of 7. The experimental results are well explained by numerical simulations of a foil plasma with a preformed plasma and analytical evaluations considering the plasma expansion.

DOI: 10.1103/PhysRevAccelBeams.21.041302

Intense ultrashort electron pulses are driven by the interaction of intense short laser pulses with solid targets. Laser-accelerated fast electrons have many possible applications, such as fast ignition for inertial confinement fusion [1,2], ultrafast electron diffraction measurement [3,4], and ultrafast transient field measurement [5,6], because of their higher absorptance of the laser pulse. The efficient transport of laser-accelerated electrons is important for these applications. For example, in the fast ignition scheme for laser fusion, numerous studies have examined the transport of fast electrons into the compressed fuel core [7–9]. In other applications using fast electrons as probe pulses with high temporal resolution, it is desirable for a greater number of electrons to be emitted from the laser plasma. For example, an ultrafast electron pulse with an energy of 350 keV and duration of 500 fs has been produced with intense laser acceleration and its application to ultrafast electron diffraction or dynamical measurement of surface plasmon polaritons has been proposed. Increasing the number of electrons per pulse is essential for obtaining useful data. Increasing the energy of the incident laser pulse increases the number of electrons escaping from the solid target (escaping electrons) [10]. This can also be achieved by increasing the absorptance of the incident laser energy, for example by controlling a preformed plasma or target surface structure [11–14]. There are also many studies of controlling the divergence of the emitted electrons, which increases the number of available electrons [15–18]. However, most laser-accelerated electrons cannot escape from the laser plasma because they are trapped by a strong quasistatic electric field, called the sheath field, produced around the steep density gradient boundary between the solid/plasma and the vacuum [19,20]. Furthermore, theoretical work shows that the fraction of fast electrons escaping from the laser plasma decreases as the initial target size decreases because the fast electrons are trapped by their own potential [21]. Almost all electrons are bound within the solid target, and only about 1% of the hot electrons can escape [10,22]. Therefore, only a small fraction of electrons accelerated by intense short-pulse laser radiation escapes from the laser plasma, and most of the electrons expend their energy heating the target or producing other types of radiation.

Suppressing the sheath fields and reflection at the boundary increases the number of escaping electrons. Zhou *et al.* used a subnanosecond laser pulse to produce a strong toroidal magnetic field, which collimated the fast electrons generated by a subpicosecond intense laser pulse [17]. They also observed that suppressing the sheath field increased the number of escaping electrons. For the fast electrons to reach far enough from the target as escaping electrons and not return to the laser plasma and reach the detectors, however, the potential produced by fast electrons must also be decreased [21]. It was predicted that the potential depends on the number of accelerated electrons, temperature, and initial target size. Therefore, it is vital to investigate the potential to understand the behavior of

*Corresponding author.

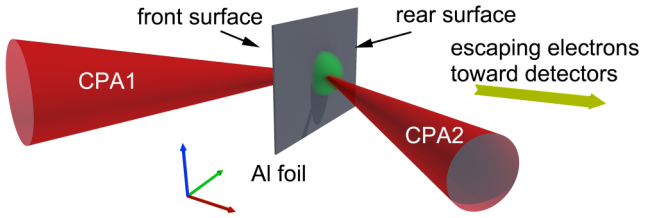

FIG. 1. Schematic of the experimental setup. Two laser pulses (CPA1 and CPA2) are focused on the Al target (thickness: 11 μm).

escaping electrons. Here, we demonstrate the intensification of electrons escaping from an intense laser plasma by using double femtosecond laser pulses. An intense pulse from a chirped pulse amplification laser (CPA1) for driving fast electrons is used to irradiate a foil target, the rear of which is preirradiated with another laser pulse (CPA2). Preirradiation with CPA2 controls the electron density distributions in the target to suppress sheath field growth and expand the target plasma into which the fast electrons are released. The number of escaping electrons increases greatly when the target is irradiated with CPA2 540 ps prior to CPA1. The number of escaping electrons with an energy of 380 keV released into vacuum is 7 times that for single-pulse irradiation. These results are supported by two-dimensional (2D) particle-in-cell (PIC) simulations of plasma produced by CPA2 and analytical evaluation considering the expansion of the plasma. These results show that over 10% of the accelerated electrons will be converted to escaping electrons by controlling the expanding plasma.

The experiments were carried using a Ti:sapphire CPA system (center wavelength: 810 nm; pulse width: 60 fs; pulse energy: 450 mJ) at Kyoto University. Laser pulses are split into CPA1 for accelerating fast electrons and CPA2 for preirradiation (Fig. 1). The CPA1 laser pulse is focused onto the front of an aluminum foil target with p-polarization at an incidence angle of 45°. The focal spot size is measured to be 7×4 μm (full width at half maximum; FWHM) with a peak intensity of 1×10^{18} W cm^{-2}. The CPA2 laser pulse is focused onto the surface of the rear of the target, the opposite side to the CPA1-irradiated surface, with p-polarization at an incidence angle of 45°. The focal spot size is measured as 50×30 μm (FWHM) with a peak intensity of 2×10^{15} W cm^{-2}. The intensity of the CPA2 pulse is selected to create an appropriate size of the additional plasma without perturbing the front surface. The time interval between CPA1 and CPA2 is varied from −540 to 130 ps. The zero delay time is determined to within ±500 fs through a cross-correlation measurement using two electron pulses [23]. The energy spectrum and beam profile of the electrons escaping from the rear side of the target to the vacuum are measured separately by a magnetic spectrometer and an electron imaging system [24], respectively. The electron imaging system is composed of an electron lens, a fluorescent screen, and an electron-multiplying charged coupled device (EM-CCD) camera. The electrons emitted normal to the target foil are focused by the electron lens with a solid angle of 5.8×10^{-5} sr onto the fluorescent screen. The energy of the electrons imaged on the screen is selected by the electron lens, and it is found to be 380 keV by measuring the diffraction from a gold single crystal. The sensitivity of the imaging system, including the electron lens, fluorescent screen, EM-CCD camera, and EM-CCD camera imaging lens, to 380 keV electrons is calibrated by using imaging plates.

A large increase in the total kinetic energy of electrons (up to a factor of 3) is observed as the time interval between the CPA1 and CPA2 pulses is increased (Fig. 2). The time interval is called the time delay relative to the time origin of CPA1. Therefore, a negative delay means that the CPA2 pulse arrives before the CPA1 pulse. The energy spectrum is almost unchanged for time delays greater than −6.7 ps. In contrast, for a time delay of less than −73 ps, the number of escaping electrons with an energy of less than 1 MeV increases with the time delay. The total kinetic energy of the escaping electrons measured by the magnetic spectrometer increases by a factor of 3 at a time delay of −540 ps (inset of Fig. 2). Only electrons with energies of less than 1 MeV are affected by the CPA2 irradiation. The slope temperature, T_{slope}, of about 270 keV is not affected by the CPA2 irradiation at any time delay. The values of T_{slope} are obtained by fitting the energy spectrum with $A\exp(-E/T_{\mathrm{slope}})$ for energies higher than 1 MeV, where A is the electron number density at $E = 0$ and E is the energy of the electrons. This result suggests that electrons with lower energy that are reflected by the sheath field without the CPA2 irradiation can escape from the laser plasma generated by the CPA2 irradiation. Because the slope temperature is constant, it is

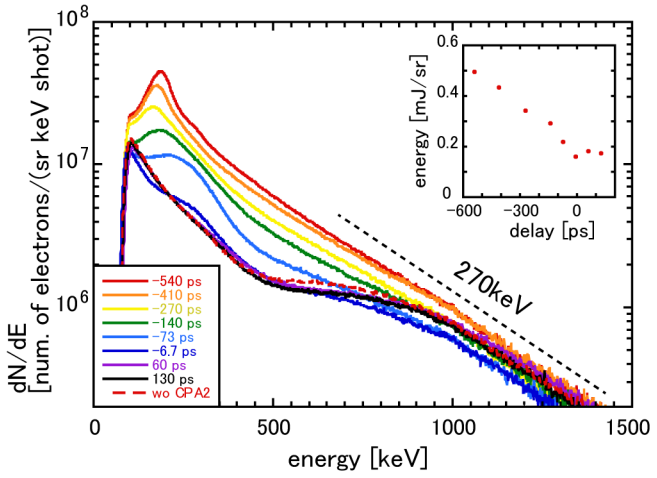

FIG. 2. Dependence of the electron energy spectrum on time delay. Spectra are obtained by averaging 100 shots. The energy spectrum without the CPA2 pulse is almost the same as those for positive time delay. The inset shows the time-delay dependence of the amount of electron energy as measured by the magnetic spectrometer. The deviation of the electron energy is about 20%.

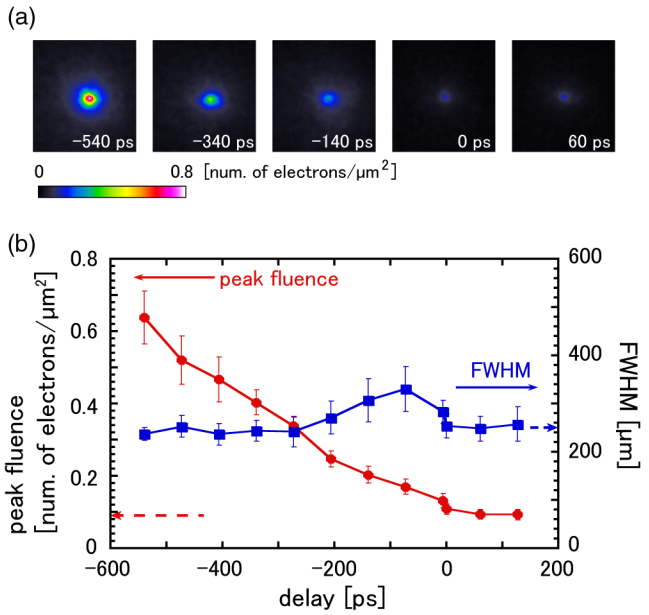

FIG. 3. (a) Images of the electron sources at time delays of −540, −340, −140, 0, and 60 ps. (b) Dependence of electron beam intensity on time delay. Error bars represent standard deviations. Dashed arrows show the results obtained by irradiation with the CPA1 pulse alone.

suspected that preformed plasma produced by the CPA2 pulse at the front of the target is negligible and the absorption of the CPA1 pulse is hardly affected by the CPA2 pulse.

We also demonstrate a substantial increase in the beam intensity of the fast electrons by using the electron lens. The energy of the fast electrons is selected to be 380 keV by the electron lens. Figure 3(a) shows single-shot images obtained by the electron imaging system at time delays of −540, −340, −140, 0, and 60 ps. Here, the intensity and focal position of the CPA1 and CPA2 pulses are carefully adjusted to increase the intensity of the electron beam, the intensity of which is increased while the spot size is kept constant when the optical delay is less than −100 ps. The electron beam with energy below 200 keV (peak at Fig. 2) is also measured with another electron lens. The beam contains a large number of electrons but has a large beam size and low peak intensity. Figure 3(b) shows the dependence on time delay of the electron beam intensity and size on the fluorescent screen. Each point is obtained by averaging over 20 laser shots. The laser focusing position and intensity are not changed while changing the time delay. These parameters are optimized only once before the measurements. Dashed arrows in Fig. 3(b) show the results obtained by irradiation with the CPA1 pulse alone. The peak count increases as the time delay decreases and a substantial increase appears only when the time delay is negative. At a time delay of −540 ps, the number of electrons in the FWHM spots is 7 times higher than that obtained by irradiation with the CPA1 pulse alone. We obtain the increased electron beam intensity while maintaining the lateral profile at an optical delay of less than −200 ps, which indicates that the electron bunch is not distorted by the plasma on the rear side or compression of the target. Although the number of electrons is still increasing as the time delay decreases, the number may be saturated or have reached a peak, depending on the laser conditions.

As shown in Figs. 2 and 3, the CPA2 pulse irradiation on the target rear surface strongly affects the number of escaping electrons. The increase in the number of escaping electrons occurs on a subnanosecond timescale. For the CPA2 pulse irradiation, no fast electrons are detected by the spectrometer and the electron imaging system. These results strongly suggest that the modulation of the electron density distributions in the target caused by the CPA2 pulse affects the transport of the fast electrons. The pulse duration of the CPA2 is ultrashort (femtosecond timescale); thus, there is no large temperature gradient on the subnanosecond timescale. It is assumed that a toroidal magnetic field, which can collimate fast electrons [17], is not created. The angular distributions of the escaping electrons for each time delay are also measured separately with imaging plates. The efficient increase of the number of escaping electrons was shown in the target normal direction. These features can be explained by two mechanisms: suppression of the growth of the sheath field due to the disappearance of the steep density gradient, and expansion of the target plasma into which the fast electrons are released. To verify these assumptions, we measure the spatial distributions of the electron density produced by the CPA2 pulse with a modified Nomarski interferometer [25] and perform 2D PIC simulations. The temporal evolution of the electron density distributions along the target normal direction measured with the interferometer is shown in Fig. 4 with

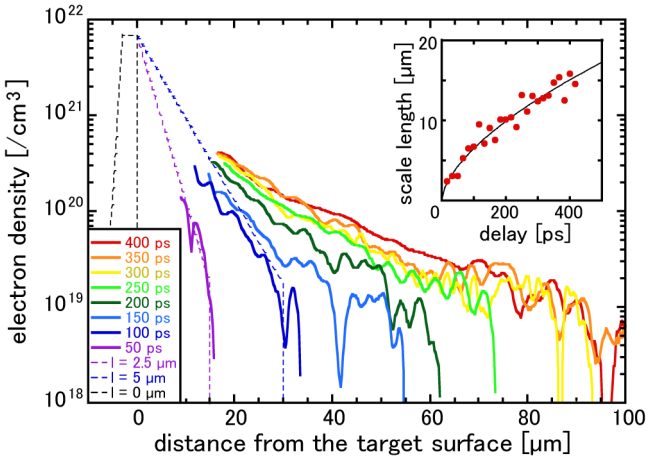

FIG. 4. Evolution of electron density distribution (solid lines). The inset shows an expansion of the scale length versus time obtained by fitting the electron density distribution for various time delays. Dashed lines show the electron density distributions with scale lengths of 0, 2.5, and 5 μm used for the 2D PIC simulations.

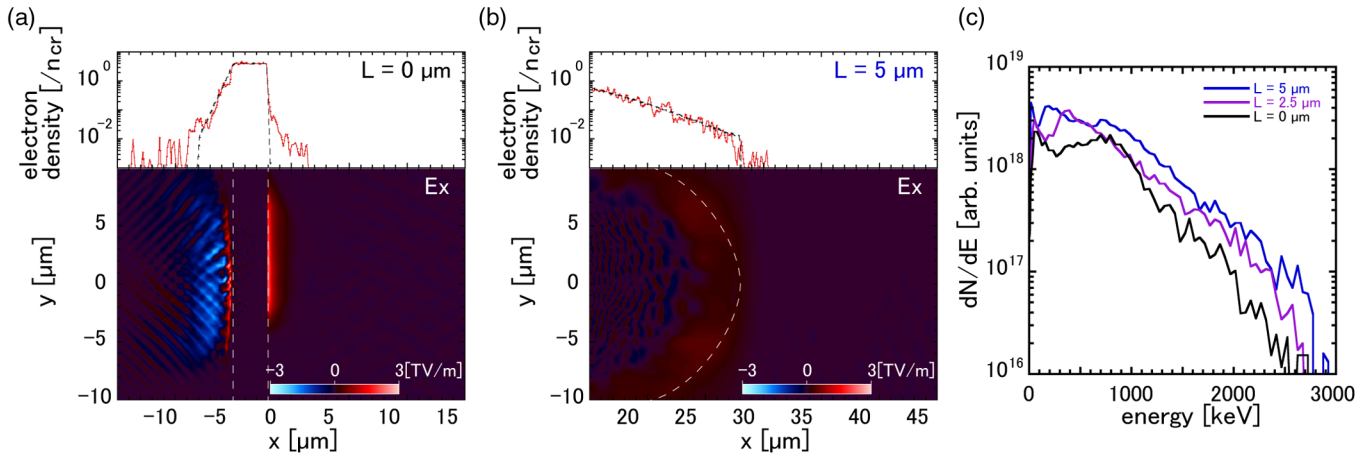

FIG. 5. PIC simulation results for the distribution of the electric field (E_x) and cross section of the electron density distributions at $y = 0$, for (a) $L = 0$ μm and (b) $L = 5$ μm at the time when the electrons passed the plasma boundary. Dashed lines show the boundaries of the plasma for $t = 0$. (c) Energy spectrum of the escaping electrons at $x = 60$ μm and -60 μm $< y <$ 60 μm.

solid lines. The distributions show cross sections at the center of the focal position. We use an aluminum wire with a diameter of 1 mm and irradiate the wire with the CPA2 pulse because accurate interference measurements can be obtained if the target surface has a slight curvature. The difference in the thickness of the target does not affect the density distributions because separate measurements showed that no holes form in the target foil over 100 ns from irradiation with the CPA2 pulse. A probe pulse is obtained by splitting a small fraction from the CPA2 pulse and doubling its frequency. The CPA2 spot is elliptical instead of circular; thus, we assume that the density distribution reflects the CPA2 focal profile and reconstruct the density distribution with an elliptical Abel inversion [26]. The plasma sizes are evaluated with an exponential density profile, $\rho = \rho_0 \exp(-x/L)$, where x is the distance from the target surface, ρ_0 is the intercept at $x = 0$, and L is the scale length.

We performed numerical simulations considering the initial plasma density profile with the 2D PIC code FISCOF2 [27]. In the simulations, p-polarized laser pulses are irradiated onto plasmas at an incidence of 45° in the $x - y$ plane. The spatial and temporal distributions of the incident laser pulses are Gaussian, and the pulse durations and spot sizes are 40 fs and 5 μm (FWHM), respectively, corresponding to an intensity of 4×10^{18} W cm^{-2}. The front surfaces of the plasmas have a scale length of 2 μm and a thickness of 3 μm with $4.0n_c$, where $n_c = 1.7 \times 10^{21}$ cm^{-3}. Null, semispherical, and semiellipsoidal plasmas are placed at the rear surface. The plasmas have radial scale lengths of 0, 2.5, and 5 μm, respectively. The cross sections of these initial plasma density profiles are shown in Fig. 4 with dashed lines. The initial electron and ion (Al^+) temperatures are 0.1 keV and 3 eV, respectively. Figures 5(a) and 5(b) show the electron density distributions at $y = 0$, where y is parallel to the plasma surface, and the spatial electric field distributions for scale lengths of 0 and 5 μm for two different times relative to the passing of the front edge of the electrons, the width of which is about 10 fs (corresponding to 3 μm), at the plasma boundary. For $L = 0$ [Fig. 5(a)], there is a strong quasistatic electric field reaching up to 3 TV/m at the target rear surface with an exponential decrease at a decay constant of 2 μm^{-1}, and electrons are subsequently reflected or lose energy because of this electric field. In contrast, when $L = 5$ μm [Fig. 5(b)], the growth of the electric field is suppressed by the rear plasma. To investigate the dependence of the rear-side plasma on the escaping electrons, we analyze the energy spectrum of the escaping electrons at $x = 60$ μm and -60 μm $< y <$ 60 μm [Fig. 5(c)]. The number of electrons below 800 keV increases by a factor of 2 for the plasma target, while the slope temperatures for any L at energies above 1 MeV are equal. Although the solid angle of the detector differs between the experiments and the simulations, the features of the energy spectra simulated by the PIC calculations agree well with those of the experimental spectra. This indicates that the number of escaping electrons increases because the sheath field disappears.

The number of escaping electrons increases with increasing time delay; that is, there is expansion of the target plasma into which the fast electrons are released (insets of Figs. 2 and 3). The size of the plasma is shown in the inset of Fig. 4 with the scale length. To explain the dependence of the number of escaping electrons on time delay, we apply a simple model proposed by Fill [21] and used by Quinn *et al.* [22]. When Maxwellian electrons are released from an initially neutral sphere of radius r_0, the fraction of electrons, ξ_∞, that can escape from the potential they produce may be estimated by

$$\frac{\ln \xi_\infty}{\xi_\infty} = -\frac{r_c}{r_0}\frac{m_e c^2}{k_B T_h} N_{\text{total}},$$

where r_0 is the classical electron radius, m_e is the electron mass, c is the speed of light, $k_B T_h$ is the hot electron

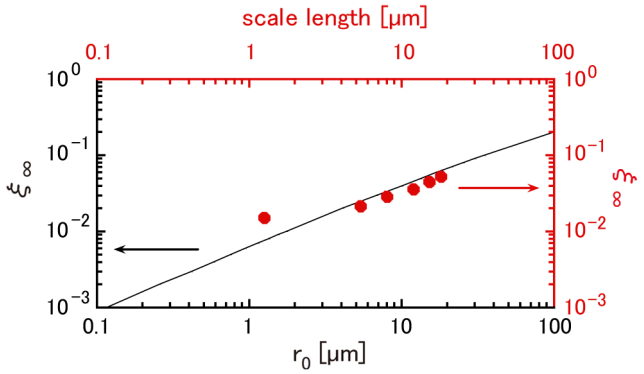

FIG. 6. Fraction of escaping electrons as a function of initial plasma radius obtained from the model calculation (solid line) and as a function of scale length (circles). The deviations of the fractions calculated from Fig. 2 are about 20%.

temperature, and N_{total} is the number of fast electrons. In Fig. 6, the solid line shows the electron fractions versus the radius of an initially neutral sphere. We use the fast electron temperature of 270 keV for $k_B T_h$ based on the experimental results (Fig. 2) and assume that the rate of absorption of the laser energy into the fast electrons is 10% to estimate N_{total} [28]. This model calculation indicates that the fraction of electrons increases with the initial plasma radius. The measurement data are also shown in Fig. 6 with circles. For these plots, we use N_{total} in the same manner as in the model calculation and use a divergence angle of 30° for the fast electrons released into the plasma [29]. The Debye length of the plasma produced by the CPA2 pulse is estimated to be sufficiently smaller than the scale length. It still unclear whether there is agreement in terms of absolute values because we do not measure or estimate the rate of absorption and the divergence angle in our experimental conditions. However, the increase in the fraction of electrons with the size of the plasma agrees well, indicating that controlling the plasma into which fast electrons are released is important for increasing the number of escaping electrons available for use. With plasma at the rear surface with scale lengths over 35 μm, the fraction of escaping electrons exceeds 0.1. To obtain such a large scale length, a longer time delay or higher intensity of CPA2 may be effective. To optimize the conditions, we must investigate in greater detail over a wider range of parameters, for example, target material, thickness, delay, and CPA1 and CPA2 intensities.

In summary, we have demonstrated a substantial increase in the number of escaping electrons from an intense laser plasma by producing an adequate plasma on the opposite surface to the intense laser irradiation. 2D PIC simulations and a model calculation also suggested that the large increase in electron beam intensity resulted from suppressing the growth of the sheath field because the steep density gradient disappeared and the target plasma into which the fast electrons were released expanded. These results show that the intense laser-irradiated foil could be used as a plasma-attached cathode, with great potential for high-brightness electron guns. The interaction of the intense laser with a solid target has a higher absorptance of the laser pulse. Compared with using a gas target, using a solid target would facilitate a laser with a higher repetition rate, and ultimately, faster electrons offer more potential to develop applications. This work contributes to the understanding of laser-plasma physics and to the development of advanced applications based on ultrafast electron pulses.

This work was supported by a Grant-in-Aid for Challenging Exploratory Research (Grant No. 25600138), a Grant-in-Aid for Scientific Research (S) (Grant No. 23226002), a Grant-in-Aid for Scientific Research (A) (Grant No. 16H02127), a Grant-in-Aid for Young Scientists (B) (Grants No. 26800280 and No. 16K17845), the Yamada Science Foundation, the Mitsubishi Foundation, and the Matsuo Foundation.

[1] M. Tabak, J. Hammer, M. E. Glinsky, W. L. Kruer, S. C. Wilks, J. Woodworth, E. M. Campbell, M. D. Perry, and R. J. Mason, Ignition and high gain with ultrapowerful lasers, Phys. Plasmas **1**, 1626 (1994).

[2] S. Atzeni, Inertial fusion fast ignitor: Igniting pulse parameter window vs the penetration depth of the heating particles and the density of the precompressed fuel, Phys. Plasmas **6**, 3316 (1999).

[3] S. Tokita, S. Inoue, S. Masuno, M. Hashida, and S. Sakabe, Single-shot ultrafast electron diffraction with a laser-accelerated sub-MeV electron pulse, Appl. Phys. Lett. **95**, 111911 (2009).

[4] S. Tokita, M. Hashida, S. Inoue, T. Nishoji, K. Otani, and S. Sakabe, Single-Shot Femtosecond Electron Diffraction with Laser-Accelerated Electrons: Experimental Demonstration of Electron Pulse Compression, Phys. Rev. Lett. **105**, 215004 (2010).

[5] S. Tokita, S. Sakabe, T. Nagashima, M. Hashida, and S. Inoue, Strong sub-terahertz surface waves generated on a metal wire by high-intensity laser pulses, Sci. Rep. **5**, 8268 (2015).

[6] S. Inoue, S. Tokita, M. Hashida, and S. Sakabe, Transient changes in electric fields induced by interaction of ultraintense laser pulses with insulator and metal foils: Sustainable fields spanning several millimeters, Phys. Rev. E **91**, 043101 (2015).

[7] R. Kodama *et al.*, Plasma devices to guide and collimate a high density of MeV electrons, Nature (London) **432**, 1005 (2004).

[8] S. Kar, A. P. L. Robinson, D. C. Carroll, O Lundh, K. Markey, P. McKenna, P. Norreys, and M. Zepf, Guiding of Relativistic Electron Beams in Solid Targets by Resistively Controlled Magnetic Fields, Phys. Rev. Lett. **102**, 055001 (2009).

[9] G. Chatterjee, P. K. Singh, S. Ahmed, A. P. L. Robinson, A. D. Lad, S. Mondal, V. Narayanan, I. Srivastava, N. Koratkar, J. Pasley, A. K. Sood, and G. Ravindra

Kumar, Macroscopic Transport of Mega-ampere Electron Currents in Aligned Carbon-Nanotube Arrays, Phys. Rev. Lett. **108**, 235005 (2012).

[10] G. Malka and J. L. Miquel, Experimental Confirmation of Ponderomotive-Force Electrons Produced by an Ultrarelativistic Laser Pulse on a Solid Target, Phys. Rev. Lett. **77**, 75 (1996).

[11] A. G. Mordovanakis, J. Easter, N. Naumova, K. Popov, P.-E. Masson-Laborde, B. Hou, I. Sokolov, G. Mourou, I. V. Glazyrin, W. Rozmus, V. Bychenkov, J. Nees, and K. Krushelnick, Quasimonoenergetic Electron Beams with Relativistic Energies and Ultrashort Duration from Laser-Solid Interactions at 0.5 kHz, Phys. Rev. Lett. **103**, 235001 (2009).

[12] K. A. Ivanov, S. A. Shulyapov, P. A. Ksenofontov, I. N. Tsymbalov, R. V. Volkov, A. B. Savel'ev, A. V. Brantov, V. Yu. Bychenkov, A. A. Turinge, A. M. Lapik, A. V. Rusakov, R. M. Djilkibaev, and V. G. Nedorezov, Comparative study of amplified spontaneous emission and short pre-pulse impacts onto fast electron generation at subrelativistic femtosecond laser-plasma interaction, Phys. Plasmas **21**, 093110 (2014).

[13] D. Margarone, O. Klimo, I. J. Kim, J. Prokůpek, J. Limpouch, T. M. Jeong, T. Mocek, J. Pšikal, H. T. Kim, J. Proška, K. H Nam, L. Štolcová, I. W. Choi, S. K. Lee, J. H. Sung, T. J. Yu, and G. Korn, Laser-Driven Proton Acceleration Enhancement by Nanostructured Foils, Phys. Rev. Lett. **109**, 234801 (2012).

[14] T. Ceccotti *et al.*, Evidence of Resonant Surface-Wave Excitation in the Relativistic Regime through Measurements of Proton Acceleration from Grating Targets, Phys. Rev. Lett. **111**, 185001 (2013).

[15] Y. T. Li, X. H. Yuan, M. H. Xu, Z. Y. Zheng, Z. M. Sheng, M. Chen, Y. Y. Ma, W. X. Liang, Q. Z. Yu, Y. Zhang, F. Liu, Z. H. Wang, Z. Y. Wei, W. Zhao, Z. Jin, and J. Zhang, Observation of a Fast Electron Beam Emitted along the Surface of a Target Irradiated by Intense Femtosecond Laser Pulses, Phys. Rev. Lett. **96**, 165003 (2006).

[16] R. H. H. Scott *et al.*, Controlling Fast-Electron-Beam Divergence Using Two Laser Pulses, Phys. Rev. Lett. **109**, 015001 (2012).

[17] H. B. Zhuo, Z. L. Chen, Z. M. Sheng, M. Chen, T. Yabuuchi, M. Tampo, M. Y. Yu, X. H. Yang, C. T. Zhou, K. A. Tanaka, J. Zhang, and R. Kodama, Collimation of Energetic Electrons from a Laser-Target Interaction by a Magnetized Target Back Plasma Preformed by a Long-Pulse Laser, Phys. Rev. Lett. **112**, 215003 (2014).

[18] H. Nakajima, S. Tokita, S. Inoue, M. Hashida, and S. Sakabe, Divergence-Free Transport of Laser-Produced Fast Electrons Along a Meter-Long Wire Target, Phys. Rev. Lett. **110**, 155001 (2013).

[19] A. J. Mackinnon, Y. Sentoku, P. K. Patel, D. W. Price, S. Hatchett, M. H. Key, C. Andersen, R. Snavely, and R. R. Freeman, Enhancement of Proton Acceleration by Hot-Electron Recirculation in Thin Foils Irradiated by Ultraintense Laser Pulses, Phys. Rev. Lett. **88**, 215006 (2002).

[20] S. Buffechoux *et al.*, Hot Electrons Transverse Refluxing in Ultraintense Laser-Solid Interactions, Phys. Rev. Lett. **105**, 015005 (2010).

[21] E. E. Fill, Ultrashort-pulse laser plasmas: Fraction of hot electrons escaping from the target and electron spectra in planar and spherical geometry, Phys. Plasmas **12**, 052704 (2005).

[22] K. Quinn *et al.*, Laser-Driven Ultrafast Field Propagation on Solid Surfaces, Phys. Rev. Lett. **102**, 194801 (2009).

[23] S. Inoue, S. Tokita, K. Otani, M. Hashida, M. Hata, H. Sakagami, T. Taguchi, and S. Sakabe, Autocorrelation Measurement of Fast Electron Pulses Emitted through the Interaction of Femtosecond Laser Pulses with a Solid Target, Phys. Rev. Lett. **109**, 185001 (2012).

[24] S. Inoue, S. Tokita, T. Nishoji, S. Masuno, K. Otani, M. Hashida, and S. Sakabe, Single-shot microscopic electron imaging of intense femtosecond laser-produced plasmas, Rev. Sci. Instrum. **81**, 123302 (2010).

[25] R. Benattar, C. Popovics, and R. Sige, Polarized light interferometer for laser fusion studies, Rev. Sci. Instrum. **50**, 1583 (1979).

[26] S. Himeno, M. Seki, H. Mochizuki, T. Enoto, and T. Sekiguchi, Computer method for new elliptical Abel inversion applied to holographic plasma diagnostics, J. Phys. Soc. Jpn. **54**, 1737 (1985).

[27] H. Sakagami and K. Mima, in *Proceedings of the 2nd International Conference on Inertial Fusion Science and Applications, Kyoto, 2001* (Elsevier, New York, 2002), pp. 380–383.

[28] J. R. Davies, Laser absorption by overdense plasmas in the relativistic regime, Plasma Phys. Controlled Fusion **51**, 014006 (2009).

[29] J. S. Green *et al.*, Effect of Laser Intensity on Fast-Electron-Beam Divergence in Solid-Density Plasmas, Phys. Rev. Lett. **100**, 015003 (2008).